APCOM'07 in conjunction with EPMESC XI, *December 3-6, 2007, Kyoto, JAPAN*

A Finite Element Method Using Node-Based Interpolation

Worsak Kanok-Nukulchai*, Foek Tjong Wong

School of Engineering and Technology, Asian Institute of Technology, P.O. Box 4, Klong Luang, Pathumthani, 12120, Thailand
e-mail: worsak@ait.ac.th, WongFoek.Tjong@ait.ac.th,

Abstract During the past two decades, a large variety of mesh-free methods have been introduced as superior alternatives to the traditional FEM. However, the acceptance in professional practices seems to be slow due to their implementation complexities. Recently, the authors proposed a very convenient implementation of Element-free Galerkin Method (EFGM) using the node-based Kriging interpolation (KI). Two key properties of KI are *Kronecker delta* and *consistency* properties. Due to the former, KI passes through all the nodes thus requiring no special treatment for boundary conditions. The consequence of the latter ensures reproduction of a linear interpolation if the basis function includes the constants and linear terms. In this study, layers of finite elements around any node are adopted as its domain of influence. This method is referred to as Kriging-based FEM (K-FEM), which can be viewed as a generalized form of FEM. Precisely, if we limit the nodal domain of influence to only one finite element layer around the node, K-FEM specializes to the traditional FEM.

In this study, the K-FEM was tested with 2D elastostatic, Reissner-Mindlin's plate and shell problems. The tests have been performed to investigate various important issues, including shear locking, patch test, convergence and accuracy. The tests also reveal that higher order basis function together with quartic spline (QS) correlation function can be effective in alleviating shear locking difficulty. K-FEM passes the weak patch test and therefore its convergence is guaranteed. In all cases, exceptionally accurate displacement and stress fields can be achieved in relatively coarse meshes. In addition, the same set of Kringing interpolation functions can be used to interpolate the mesh geometry. This property is particularly useful to model curved shells.

The distinctive advantage of the K-FEM is its inheritance of the computational procedure of FEM. The formulation and implementation of the method are similar to those of the standard FEM. Any existing FE code can be easily extended to K-FEM; thus, the method has a higher chance to be accepted in practice.

Key words: finite element, Kriging interpolation, element-free Galerkin method

INTRODUCTION

In the last two decades, different mesh-free methods have been developed and applied to solve academic problems in continuum mechanics (e.g., see [1], [2]). Of all the mesh-free methods, the methods using the Galerkin weak form such as the element-free Galerkin method (EFGM) [3] and point interpolation methods [1: pp.250-300] have the same basic formulation with FEM. The common advantages of these methods are: 1) there is no need for mesh for construction of shape functions; 2) high order shape functions can be easily achieved; and 3) the solutions are usually more accurate and smooth than the FEM. Although the EFGM and its variants have the abovementioned advantages and many ariticles have appeared for more than one decade, they do not seem to find wide acceptance in real practices. This is partially due to the inconvenience in its implementation, such as difficulties in satisfying essential boundary conditions and in handling problems with different material properties [1: pp.15 and 644].

Recently, a more convenient implementation of EFGM was proposed [4]. Following the work of Gu [5], Kriging interpolation (KI) is used as the trial function. Possessing Kronecker delta property, KI passes through the nodes; thus, there is no need for special treatment of boundary conditions. For implementing the integration of the Galerkin weak form, the finite elements are used as the integration cells. In this study, the KI is established for each element using a set of nodes in a domain of influence (DOI) composed of several layers of elements, *i.e.,* in the form of polygon for 2D problems. This variant of EGFM can be viewed as an enhancement of the FEM with Kriging shape functions. In this paper, this method is referred to as *Kriging-based FEM* (K-FEM).

The K-FEM retains the advantages of mesh-free methods as follows [4]: 1) any requirement for high order shape functions can be easily fulfilled without any change to the element structure, 2) the field variables and their derivatives can be obtained with remarkable accuracy and global smoothness. A distinctive advantage of the K-FEM over other mesh-free methods is that it inherits the computational procedure of FEM so that existing general-purpose FE programs can be easily extended to include this new concept. Thus, the K-FEM has a higher change to be accepted in practices. The current trend in research in the K-FEM is towards extension and application of this new technique to different problems in engineering, such as applications to beams, plates ([6], [7]) and shells, problems with material discontinuity [8], and adaptive procedure [9].

In this paper, we present fundamentals of the K-FEM. The formulation of KI and the concept of layered-element DOI are reviewed. Correlation functions and their parameters are discussed. As an example of applications, the formulation and numerical tests of the K-FEM for plane-stress/plane-strain problems are presented.

KRIGING INTERPOLATION

Named after Danie G. Krige, a South African mining engineer, Kriging is a well-known geostatistical technique for spatial data interpolation in geology and mining (e.g., see [10], [11]). Using this interpolation, every unknown value at a point can be interpolated from known values at scattered points in its specified neighborhood.

Formulation

Consider a continuous field variable $u(\mathbf{x})$ defined in a domain Ω. The domain is represented by a set of properly scattered nodes $\mathbf{x}_i$, i=1, 2, …, N, where N is the total number of nodes in the whole domain. Given N field values, $u(\mathbf{x}_1)$, …, $u(\mathbf{x}_N)$, the problem of interest is to obtain an estimate value of u at a point $\mathbf{x}_0 \in \Omega$.

The Kriging estimated value $u^{\mathrm{h}}(\mathbf{x}_0)$ is a linear combination of $u(\mathbf{x}_1)$, …, $u(\mathbf{x}_n)$, i.e.

$$u^{\mathrm{h}}(\mathbf{x}_0) = \sum_{i=1}^{n} \lambda_i u(\mathbf{x}_i) \tag{1}$$

where λ_i's are termed as (*Kriging*) *weights* and n is the number of nodes surrounding point $\mathbf{x}_0$ inside a sub-domain $\Omega_{\mathbf{x}0} \subseteq \Omega$. This sub-domain is referred to as DOI in this paper. Considering individual function values, $u(\mathbf{x}_1)$, …, $u(\mathbf{x}_n)$, as the realizations of random variables $U(\mathbf{x}_1)$, …, $U(\mathbf{x}_n)$, Eq. (1) can be written as

$$U^{\mathrm{h}}(\mathbf{x}_0) = \sum_{i=1}^{n} \lambda_i U(\mathbf{x}_i) \tag{2}$$

The Kriging weights are determined by requiring that the estimator $U^{\mathrm{h}}(\mathbf{x}_0)$ is *unbiased*, i.e.

$$\mathrm{E}\left[U^{\mathrm{h}}(\mathbf{x}_0) - U(\mathbf{x}_0)\right] = 0 \tag{3}$$

and *by minimizing* the variance of estimation error, $\mathrm{var}\left[U^{\mathrm{h}}(\mathbf{x}_0)-U(\mathbf{x}_0)\right]$. Using the method of Lagrange for constraint optimization problems, the requirements of minimum variance and unbiased estimator lead to the following Kriging equation system:

$$\mathbf{R}\boldsymbol{\lambda}+\mathbf{P}\boldsymbol{\mu}=\mathbf{r}(\mathbf{x}_0) \tag{4a}$$

$$\mathbf{P}^{\mathrm{T}}\boldsymbol{\lambda}=\mathbf{p}(\mathbf{x}_0) \tag{4b}$$

in which

$$\mathbf{R}=\begin{bmatrix} C(\mathbf{h}_{11}) & \dots & C(\mathbf{h}_{1n}) \\ \dots & \dots & \dots \\ C(\mathbf{h}_{n1}) & \dots & C(\mathbf{h}_{nn}) \end{bmatrix};\quad \mathbf{P}=\begin{bmatrix} p_1(\mathbf{x}_1) & \dots & p_m(\mathbf{x}_1) \\ \dots & \dots & \dots \\ p_1(\mathbf{x}_n) & \dots & p_m(\mathbf{x}_n) \end{bmatrix}; \tag{4c}$$

$$\boldsymbol{\lambda}=\begin{bmatrix}\lambda_1 & \dots & \lambda_n\end{bmatrix}^{\mathrm{T}};\quad \boldsymbol{\mu}=\begin{bmatrix}\mu_1 & \dots & \mu_m\end{bmatrix}^{\mathrm{T}} \tag{4d}$$

$$\mathbf{r}(\mathbf{x}_0)=\begin{bmatrix}C(\mathbf{h}_{10}) & C(\mathbf{h}_{20}) & \dots & C(\mathbf{h}_{n0})\end{bmatrix}^{\mathrm{T}};\quad \mathbf{p}(\mathbf{x}_0)=\begin{bmatrix}p_1(\mathbf{x}_0) & \dots & p_m(\mathbf{x}_0)\end{bmatrix}^{\mathrm{T}} \tag{4e}$$

$\mathbf{R}$ is $n\times n$ matrix of covariance between $U(\mathbf{x})$ at nodes $\mathbf{x}_1, \dots, \mathbf{x}_n$; $\mathbf{P}$ is $n\times m$ matrix of polynomial values at the nodes; $\boldsymbol{\lambda}$ is $n\times 1$ vector of Kriging weights; $\boldsymbol{\mu}$ is $m\times 1$ vector of Lagrange multipliers; $\mathbf{r}(\mathbf{x}_0)$ is $n\times 1$ vector of covariance between the nodes and the node of interest, $\mathbf{x}_0$; and $\mathbf{p}(\mathbf{x}_0)$ is $m\times 1$ vector of polynomial basis at $\mathbf{x}_0$. In Eqs. (4c) and (4e), $C(\mathbf{h}_{ij})=\mathrm{cov}\left[U(\mathbf{x}_i),U(\mathbf{x}_j)\right]$. Kriging weights $\boldsymbol{\lambda}$ can be obtained by solving the Kriging equations, Eqs. (4a) and (4b).

The expression for the estimated value u^{h} given by Eq. (1) can be rewritten in matrix form,

$$u^{\mathrm{h}}(\mathbf{x}_0)=\boldsymbol{\lambda}^{\mathrm{T}}\mathbf{d} \tag{5}$$

where $\mathbf{d}=\begin{bmatrix}u(\mathbf{x}_1) & \dots & u(\mathbf{x}_n)\end{bmatrix}^{\mathrm{T}}$ is $n\times 1$ vector of nodal values. Since the point $\mathbf{x}_0$ is an arbitrary point in the DOI, the symbol $\mathbf{x}_0$ can be replaced by symbol $\mathbf{x}$. Thus, using the usual finite element terminology, Eq. (5) can be expressed as

$$u^{\mathrm{h}}(\mathbf{x})=\mathbf{N}(\mathbf{x})\,\mathbf{d}=\sum_{i=1}^{n}N_i(x)u_i \tag{6}$$

in which $\mathbf{N}(\mathbf{x})=\boldsymbol{\lambda}^{\mathrm{T}}(\mathbf{x})$.

Two key properties of Kriging shape functions that make them suitable for FEM are *the Kronecker delta* (or *interpolation*) property and the *consistency* property ([4], [5]). Due to the former property KI exactly passes through the nodal values. The consequence of the latter property is that if the basis includes all constants and linear terms, the Kriging shape functions are able to reproduce a linear polynomial exactly.

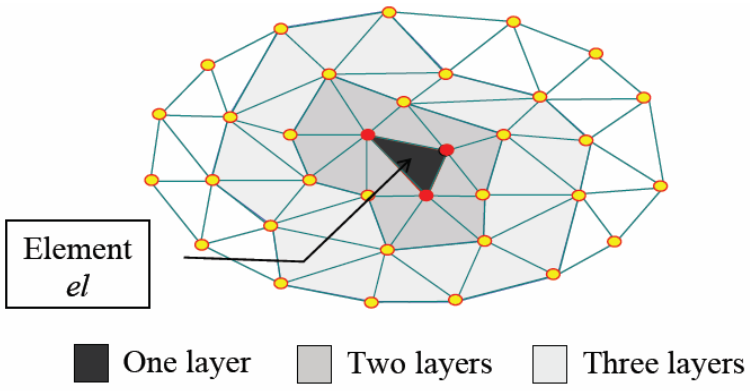

Fig. 1 Domain of influence for element el with one, two and three layers of elements [4]

Layered-Element Domain of Influence

Let us consider a 2D domain meshed with triangular elements, such as illustrated in Fig. 1. For each element, KI is constructed based upon a set of nodes in a polygonal DOI encompassing a predetermined number of layers of elements. The KI function over the element is given by Eq. (6). By combining the KI of all elements in the domain, the global field variable is approximated by piecewise KI. This way of approximation is very similar with the approximation in the conventional FEM.

It is worthy to note that it is also possible to use quadrilateral elements to implement the concept of layered-element DOI. Mesh with triangular elements is a good choice owing to its flexibility in representing complex geometry and its ease to be automatically generated.

Within each element the interpolation function is naturally continuous. However, along the element edges between two adjacent elements the function is not continuous because the KI for the edge of each neighboring element is constructed using different set of nodes. Therefore, the present method is *nonconforming*. The issue of *non-conformity* and its effects on the convergence of the solutions obtained from the K-FEM are addressed in the separate paper of the authors [12].

The number of layers for each element must cover a minimum number of nodes in such a way that the system of Kriging equations, Eqs. (4a) and (4b), can be solved. If an *m*-order polynomial basis is employed, the DOI is required to cover a number of nodes, *n*, that is equal or greater than the number of terms in the basis function [4]. Basically, it can be shown that the minimum number of layers for different polynomial bases is listed in Table 1. As the number of layers increases, the computational cost is higher. Thus the use of *minimum* number of layers for each polynomial basis is recommended.

Table 1. Minimum number of layers for various basis functions

Basis	Minimum number of layers
Linear	1
Quadratic, Bi-linear	2
Cubic, Bi-quadratic	3
Quartic, Bi-cubic	4

Polynomial Basis and Correlation Function

Constructing Kriging shape functions in Eq. (6) requires a polynomial basis function and a model of covariance function. For the basis function, besides complete polynomial bases, it is also possible to use incomplete polynomial bases such as bi-linear, bi-quadratic and bi-cubic bases [13].

Covariance between a pair of random variables $U(\mathbf{x})$ and $U(\mathbf{x}+\mathbf{h})$ can be expressed in terms of correlation coefficient function or shortly, *correlation function*, i.e. $\rho(\mathbf{h}) = C(\mathbf{h})/\sigma^2$, where $\sigma^2 = \mathrm{var}\left[U(\mathbf{x})\right]$. According to Gu [5], σ^2 has no effect on the final results and can be taken equals to 1. One of the widely used correlation model in the area of computational mechanics is the Gaussian correlation function ([4]-[9]), *viz.*

$$\rho(\mathbf{h}) = \rho(h) = \exp(-(\theta h/d)^2) \tag{7}$$

where θ>0 is the *correlation parameter*, $h = \|\mathbf{h}\|$, *i.e.* the Euclidean distance between points **x** and **x**+**h**, and *d* is a scale factor to normalize the distance. In this paper, *d* is taken to be the *largest distance* between any pair of nodes in the DOI. Besides the Gaussian, we recently introduced the quartic spline (QS) correlation function [6] as follows:

$$\rho(\mathbf{h}) = \rho(h) = \begin{cases} 1 - 6(\theta h/d)^2 + 8(\theta h/d)^3 - 3(\theta h/d)^4 & \text{for } 0 \le \theta h/d \le 1 \\ 0 & \text{for } \theta h/d > 1 \end{cases} \tag{8}$$

Our studies showed that with this correlation function, Kriging shape functions are not very sensitive to the change in parameter θ. Moreover, the convergence characteristics of the K-FEM with the QS correlation function in many cases were more satisfactory than the Gaussian function.

Figure 2 shows the plot of the Gaussian and QS correlation functions for various values of θ. It can be seen that the parameter θ determines how quickly the correlation falls off; the larger value of θ, the quicker the correlation drops. For the same value of θ, the QS function drops quicker than the Gaussian function.

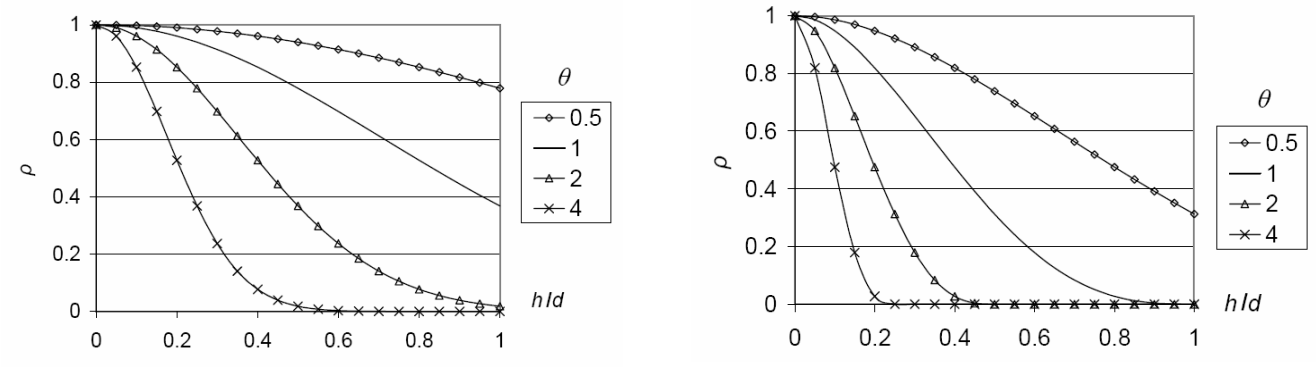

(a) (b)

Fig. 2 Correlation functions vs. normalized distance for various values of θ: (a) Gaussian, (b) quartic spline

Correlation Parameter

A proper choice of parameter θ is important as it affects the quality of KI. In order to obtain reasonable results in the K-FEM, Plengkhom and Kanok-Nukulchai [4] suggested a rule of thumb for choosing θ, i.e. θ should be selected so that it satisfies the lower bound,

$$\left| \sum_{i=1}^{n} N_i - 1 \right| \le 1 \times 10^{-10+a} \tag{9}$$

where a is the order of basis function, and also satisfies the upper bound,

$$\det(\mathbf{R}) \le 1 \times 10^{-b} \tag{10}$$

where b is the dimension of problem. For 2D problem with cubic basis function, for example, a=3 and b=2.

Numerical investigations on the upper and lower bound values of θ [6] revealed that the parameter bounds vary with respect to the number of nodes in the DOI. Based on the results of the search for the lower and upper bound values of θ that satisfy Eqs. (9) and (10), we proposed explicit parameter functions for practical implementation of the K-FEM as follows:

For the Gaussian correlation parameter, the parameter function is

$$\theta = (1-f)\theta^{\text{low}} + f\theta^{\text{up}}, \quad 0 \le f \le 0.8 \tag{11a}$$

where f is a scale factor, θ^{low} and θ^{up} are the lower and upper bound functions as follows:

$$\theta^{\text{low}} = \begin{cases} 0.08286n - 0.2386 & \text{for } 3 \le n < 10 \\ \text{-8.364E-4}\,n^2 + 0.1204n - 0.5283 & \text{for } 10 \le n \le 55 \\ 0.02840n + 2.002 & \text{for } n > 55 \end{cases} \tag{11b}$$

$$\theta^{\text{up}} = \begin{cases} 0.34n - 0.7 & \text{for } 3 \le n < 10 \\ \text{-2.484E-3}\,n^2 + 0.3275n - 0.2771 & \text{for } 10 \le n \le 55 \\ 0.05426n + 7.237 & \text{for } n > 55 \end{cases} \tag{11c}$$

For the QS correlation parameter, the parameter function can be obtained as

$$\theta = \begin{cases} 0.1329n - 0.3290 & \text{for } 3 \le n < 10 \\ 1 & \text{for } n \ge 10 \end{cases} \tag{12}$$

With these functions, *adaptive* values of θ can be used now in place of a uniform value of θ. Here, "adaptive" means that the correlation parameters used in an analysis are adjusted to the number of nodes in the DOI of each element. An advantage of the use of adaptive θ from practical viewpoint is that a user of K-FEM program is not required to input a value of θ in an analysis since its formulas can be embedded in the program.

Illustration

To illustrate further the concept of layered-element DOI and Kriging shape function, let consider a square domain as shown in Fig. 3. Using Delaunay triangulation algorithm in MATLAB version 6.5, the domain is subdivided into triangular elements of the same sizes (with seven elements on each side). Suppose that the element of interest is one of the triangular element in the center of the square, i.e. Element no.1. Its DOIs, comprising one up to four element layers, are shown in the figure. It can be seen that the DOI is not necessary to be convex.

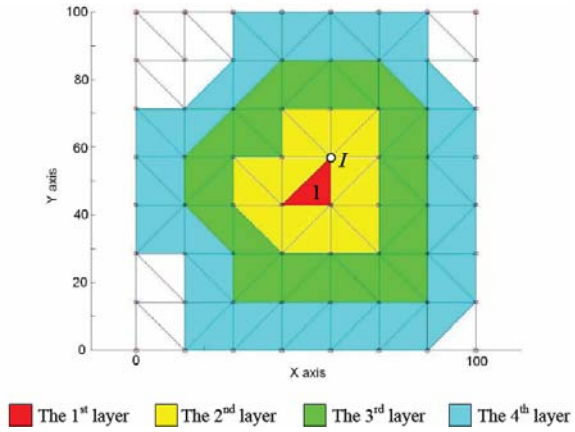

Fig. 3 Square domain with triangular elements and various layered-element domains of influence

Now suppose we use quadratic basis function (m=6) and three element layers to construct KI over Element no.1. In this case the DOI encompasses the nodes in the 1st, 2nd and 3rd layers and the total number of the nodes is 30 (n=30) as may be illustrated in Fig. 3. Hence it satisfies the requirement $n \ge m$. The plot of Kriging shape functions associated with node I, using Gaussian and QS correlation functions, is shown in Fig. 4. The correlation parameters were taken in such a way so that they are in the middle between their lower and upper bounds (Eqs. (9) and (10)), i.e. θ=4.2 for the Gaussian and θ=1.5 for the QS. One can observe that the shape function with QS correlation function is relatively more flat in the region far from the node under consideration (Node I).

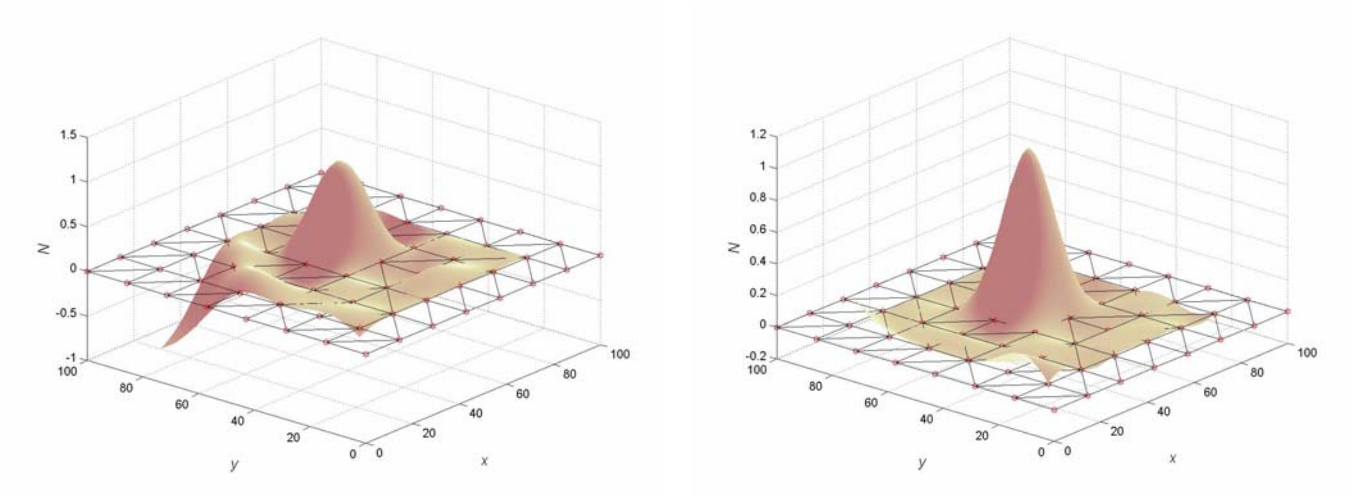

(a) (b)

Fig. 4 Kriging shape functions corresponding to node I using: (a) Gaussian correlation function, (b) quartic spline correlation function

How the shape functions change if the correlation parameter changes is demonstrated in Fig. 5. The figure shows the plot of the shape functions along line y=57.14 for 3 values of θ's, *i.e.,* at the lower bound, the midpoint, and the upper bound. It is clear from the plots that the Gaussian shape function is more sensitive to the change of θ. As θ increases, the shape function becomes less oscillating, especially at the region close to the boundary of the DOI. On the other hand, the QS shape function is not very sensitive to the change of θ. The functions for different values of θ are nearly the same, except in regions close to the boundary of the DOI. From practical point of view, the insensitivity of the shape function to the parameter θ is an advantage since a user of the K-FEM does not have to consider which value of θ should be used in the analysis.

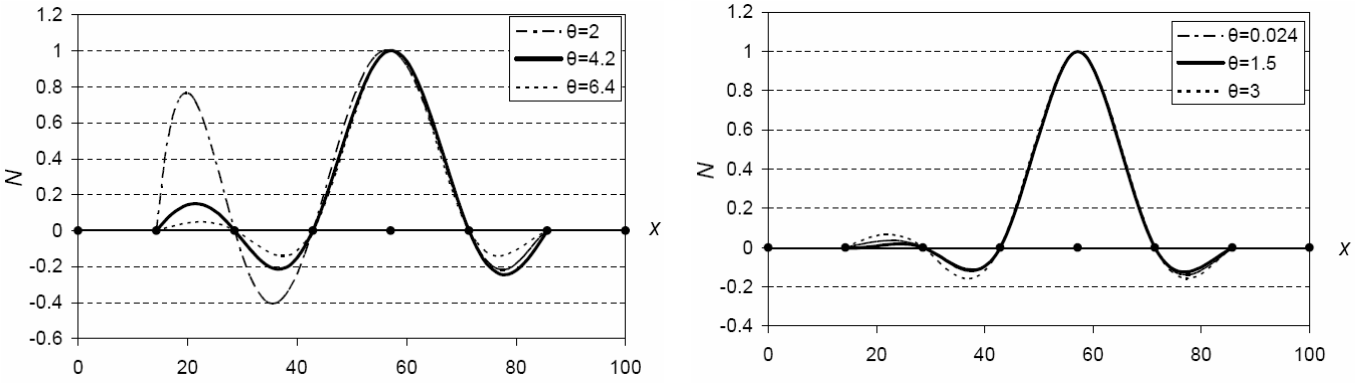

(a) (b)

Fig. 5 Kriging shape functions corresponding to node I along line y=57.14, using: (a) Gaussian correlation function, (b) quartic spline correlation function

FORMULATION OF THE K-FEM FOR 2D ELASTOSTATICS

The governing equations for 2D elastostatics in Cartesian coordinate system can be written in a weak form as follows:

$$\int_V \delta\boldsymbol{\varepsilon}^{\mathrm{T}}\boldsymbol{\sigma}\, dV = \int_V \delta\mathbf{u}^{\mathrm{T}}\mathbf{b}\, dV + \int_S \delta\mathbf{u}^{\mathrm{T}}\mathbf{t}\, dS \tag{13}$$

where $\mathbf{u} = \{u \quad v\}^{\mathrm{T}}$ is the displacement vector; $\boldsymbol{\varepsilon} = \{\varepsilon_x \quad \varepsilon_y \quad \gamma_{xy}\}^{\mathrm{T}}$ is the vector of 2D strain components; $\boldsymbol{\sigma} = \{\sigma_x \quad \sigma_y \quad \tau_{xy}\}^{\mathrm{T}}$ is the vector of 2D stress components; $\mathbf{b} = \{b_x \quad b_y\}^{\mathrm{T}}$ is the body force vector;

$\mathbf{t} = \{t_x \quad t_y\}^{\mathrm{T}}$ is the surface traction force vector; V is the 3D domain occupied by the solid body and S is the surface on which the traction $\mathbf{t}$ is applied.

Suppose the domain V is subdivided by a mesh of N_{el} elements and N nodes. To obtain an approximate solution using the concept of KI with layered-element DOI, for each element e=1, 2, …, N_{el} the displacement components u and v are approximated by the KI as follows:

$$u(x,y) \approx \sum_{i=1}^{n} N_i(x,y)\,u_i \;\; ; \quad v(x,y) \approx \sum_{i=1}^{n} N_i(x,y)\,v_i \tag{14}$$

Here, $N_i(x, y)$ denotes Kriging shape function associated with node i; u_i and v_i are nodal displacement components in the x and y directions, respectively; n is the number of nodes in the DOI of an element, which generally varies from element to element. In the matrix form, Eq. (14) may be written as

$$\mathbf{u}^e = \mathbf{N}^e \mathbf{r}^e \tag{15a}$$

where

$$\mathbf{N}^e = \begin{bmatrix} N_1 & 0 & N_2 & 0 & \cdots & N_n & 0 \\ 0 & N_1 & 0 & N_2 & \cdots & 0 & N_n \end{bmatrix} \tag{15b}$$

is the shape function matrix and

$$\mathbf{r}^e = \{u_1 \quad v_1 \quad u_2 \quad v_2 \quad \cdots \quad u_n \quad v_n\}^{\mathrm{T}} \tag{15c}$$

is the element nodal displacement vector. The variable index e is written to emphasize that the matrices are associated with element e, $1 \le e \le N_{\mathrm{el}}$, and follow the local (elemental) ordering of element e. Employing the small-strain strain-displacement relation and linear stress-strain relation and inserting the element-by-element approximation of $\mathbf{u}$, Eq. (15a), into the weak form, Eq. (13), we obtain

$$\sum_{e=1}^{N_{\mathrm{el}}} \delta\mathbf{r}^{e\mathrm{T}} \left(\int_{V^e} \mathbf{B}^{e\mathrm{T}} \mathbf{E} \mathbf{B}^e \, dV \right) \mathbf{r}^e = \sum_{e=1}^{N_{\mathrm{el}}} \delta\mathbf{r}^{e\mathrm{T}} \int_{V^e} \mathbf{N}^{e\mathrm{T}} \mathbf{b}^e \, dV + \sum_{e=1}^{N_{\mathrm{el}}} \delta\mathbf{r}^{e\mathrm{T}} \int_{S^e} \mathbf{N}^{e\mathrm{T}} \mathbf{t}^e \, dS \tag{16}$$

In this equation, $\mathbf{B}^e$ is the element strain-displacement matrix, i.e.

$$\mathbf{B}^e = \begin{bmatrix} N_{1,x} & 0 & N_{2,x} & 0 & \cdots & N_{n,x} & 0 \\ 0 & N_{1,y} & 0 & N_{2,y} & \cdots & 0 & N_{n,y} \\ N_{1,y} & N_{1,x} & N_{2,y} & N_{2,x} & \cdots & N_{n,y} & N_{n,x} \end{bmatrix} \tag{17}$$

Matrix $\mathbf{E}$ is the constitutive matrix, which for the case of isotropic material can be expressed in terms of modulus elasticity E and Poisson's ratio ν as follows:

$$\mathbf{E} = \frac{\bar{E}}{1-\bar{\nu}^2} \begin{bmatrix} 1 & \bar{\nu} & 0 \\ \bar{\nu} & 1 & 0 \\ 0 & 0 & (1-\bar{\nu})/2 \end{bmatrix} \tag{18a}$$

in which

$$\bar{E} = \begin{cases} E & \\ E/(1-\nu^2) & \end{cases} \quad \text{and} \quad \bar{\nu} = \begin{cases} \nu & \text{for plane stress} \\ \nu/(1-\nu) & \text{for plane strain} \end{cases} \tag{18b}$$

V^e is the 3D domain of element e and S^e is the surface of element e on which the traction $\mathbf{t}$ is applied. Since Eq. (16) must be true for any admissible virtual displacement $\delta\mathbf{r}^e$, we can write the equilibrium equation for each element as follows:

$$\mathbf{k}^e \mathbf{r}^e = \mathbf{R}^e \tag{19a}$$

where

$$\mathbf{k}^e = \int_{V^e} \mathbf{B}^{e\mathrm{T}}\mathbf{E}\mathbf{B}^e \, dV = t^e \int_{A^e} \mathbf{B}^{e\mathrm{T}}\mathbf{E}\mathbf{B}^e \, dA \tag{19b}$$

is the stiffness matrix of element e (the matrix dimension is $2n \times 2n$);

$$\mathbf{R}^e = \int_{V^e} \mathbf{N}^{e\mathrm{T}}\mathbf{b}^e \, dV + \int_{S^e} \mathbf{N}^{e\mathrm{T}}\mathbf{t}^e \, dS = t^e \int_{A^e} \mathbf{N}^{e\mathrm{T}}\mathbf{b}^e \, dA + t^e \int_{s^e} \mathbf{N}^{e\mathrm{T}}\mathbf{t}^e \, ds \tag{19c}$$

is the consistent nodal force vector of element e ($2n \times 1$). Here, t^e is the thickness of element e; A^e is the area domain of element e; s^e is the edge of element e.

In view of global (structural) ordering, the summation in Eq. (16) is equivalent to the finite element assembly procedure. Hence, from Eq. (16) we can obtain the global discretized equilibrium equations

$$\mathbf{K}\mathbf{r} = \mathbf{R} \tag{20a}$$

in which

$$\mathbf{K} = \mathop{\mathrm{A}}_{e=1}^{N_{\mathrm{el}}} \mathbf{k}^e \;\; ; \quad \mathbf{r} = \mathop{\mathrm{A}}_{e=1}^{N_{\mathrm{el}}} \mathbf{r}^e \;\; ; \quad \mathbf{R} = \mathop{\mathrm{A}}_{e=1}^{N_{\mathrm{el}}} \mathbf{R}^e \tag{20b}$$

Here $\mathbf{K}$ is the structural stiffness matrix ($2N \times 2N$); $\mathbf{r}$ is the structural nodal displacement vector ($2N \times 1$); $\mathbf{R}$ is the structural nodal force vector ($2N \times 1$), and $\mathop{\mathrm{A}}_{e=1}^{N_{\mathrm{el}}}$ denotes the assembly operator. It should be mentioned here that the assembly process for each element involves *all nodes in the element's DOI*, not only the nodes within the element as in the conventional FEM.

Solving Eq. (20a), one can obtain $\mathbf{r}$ and once it is known, one can extract element nodal displacement, $\mathbf{r}^e$, for each element. Stresses in each element can then be calculated by the use of the following equation:

$$\boldsymbol{\sigma}^e = \mathbf{E}\mathbf{B}^e\mathbf{r}^e \tag{21}$$

Matrix $\mathbf{B}^e$ in this equation is a function of the coordinates and must be evaluated at the locations in the element where the stresses are desired. In the following examples, the stresses are evaluated at the element nodes for every element. Subsequently, at nodes where two or more elements meet the element nodal stresses are averaged.

It is worthwhile to note that the interpolation function for calculation of the stresses do not have to be the same as that used for constructing the stiffness matrix. For example, if the KI employed to construct the stiffness matrix is Kriging with the options of quadratic basis, two-element-layer DOI, QS correlation function (P2-2-QS), the KI in evaluating the stresses may be with the options of cubic basis, three element-layers, Gaussian correlation function (P3-3-G). It is also possible to use the constant-strain-triangle interpolation function for calculation of the stresses. In the following examples, however, the interpolation function for calculation of the stresses is taken to be the same as that used for constructing the stiffness matrix.

NUMERICAL TESTS

To study the accuracy and convergence of the present K-FEM, two measures of errors are utilized. The fist one is the relative error of displacement norm, defined as

$$r_u = \left(\frac{\int_V (\mathbf{u}^{\mathrm{app}} - \mathbf{u}^{\mathrm{exact}})^{\mathrm{T}} (\mathbf{u}^{\mathrm{app}} - \mathbf{u}^{\mathrm{exact}}) \, dV}{\int_V (\mathbf{u}^{\mathrm{exact}})^{\mathrm{T}} \mathbf{u}^{\mathrm{exact}} \, dV} \right)^{1/2} \tag{22}$$

where $\mathbf{u}^{\mathrm{app}}$ and $\mathbf{u}^{\mathrm{exact}}$ are the approximate and the exact displacement vectors, respectively. The second one is the relative error of strain energy norm, defined as

$$r_\varepsilon = \left(\frac{\int_V (\boldsymbol{\varepsilon}^{\text{app}} - \boldsymbol{\varepsilon}^{\text{exact}})^{\text{T}} \mathbf{E} (\boldsymbol{\varepsilon}^{\text{app}} - \boldsymbol{\varepsilon}^{\text{exact}})\, dV}{\int_V (\boldsymbol{\varepsilon}^{\text{exact}})^{\text{T}} \mathbf{E} \boldsymbol{\varepsilon}^{\text{exact}}\, dV} \right)^{1/2} \tag{23}$$

where $\boldsymbol{\varepsilon}^{\text{app}}$ and $\boldsymbol{\varepsilon}^{\text{exact}}$ are approximate and exact strain vectors, respectively. For computing these relative errors, the 13-point quadrature rule for triangles (see *e.g.* [14: p.173]), which can give error figures of four digits accuracy, is employed.

The element stiffness matrix, Eq. (19b), is computed using the 6-point quadrature rule for triangles. The 6-point rule is selected because it can give reasonably accurate results (three digits accuracy in most cases) yet inexpensive in terms of computational cost. For computing the nodal force vector, Eq. (19c), the 2-point Gaussian quadrature for line integral is used since it results in exact nodal force vector for edge traction force with cubic distribution or less.

Abbreviations in the form of P*-*-G* or P*-*-QS, in which the star denotes a number, are adopted in this section to designate various options of the K-FEM. The first part of the abbreviation denotes polynomial basis with the order indicated by the number next to letter P; the middle part denotes number of layers; the last part, G* denotes the Gaussian correlation function with the adaptive parameter given by Eq. (11a) and with the scale factor f indicated by the number next to letter G (in percent); QS denotes the quartic spline correlation function with the adaptive parameter given by Eq. (12). For example, P3-3-G50 means cubic basis, 3 element-layers, Gaussian correlation function with mid-value parameter function, i.e. f=0.5.

A Cantilever Plane Stress Beam Example

A cantilever plane stress beam of one unit thickness subjected to parabolic end shear traction as shown in Fig. 6. The analytical solutions for this problem are as follows [15]:

$$u = -\frac{P}{6EI}\left(y - \frac{D}{2}\right)\left[3x(2L-x) + (2+\nu)y(y-D)\right] \tag{24a}$$

$$v = \frac{P}{6EI}\left[x^2(3L-x) + 3\nu(L-x)\left(y-\frac{D}{2}\right)^2 + \frac{4+5\nu}{4}D^2 x\right] \tag{24b}$$

$$\sigma_x = -\frac{P}{I}(L-x)\left(y-\frac{D}{2}\right)\ ; \quad \sigma_y = 0\ ; \quad \tau_{xy} = -\frac{Py}{2I}(y-D) \tag{24c}$$

where $I=D^3/12$.

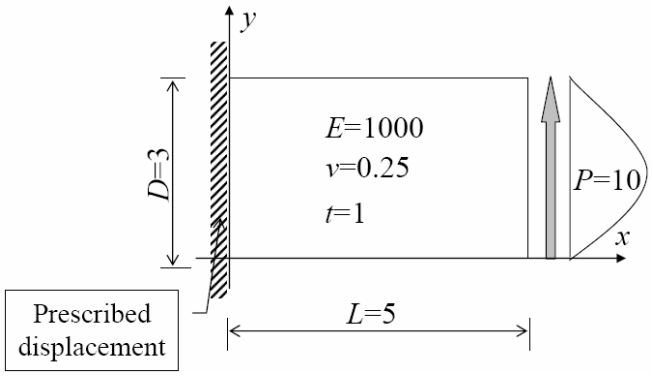

Fig. 6 A cantilever beam subjected to parabolic shear stress

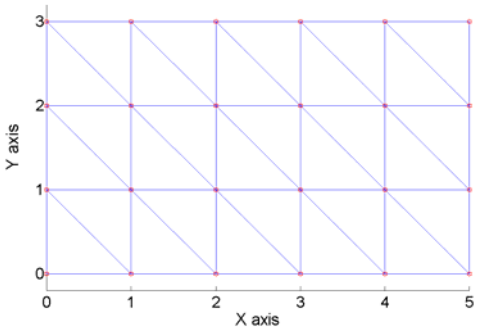

Fig. 7 Initial mesh of the cantilever beam

To study the convergence of the K-FEM with various options, the beam is modelled with different degrees of mesh refinement. The initial course mesh with 24 nodes (the element characteristic size h=1) is shown in Fig. 7. Subsequent meshes are constructed by subdividing the previous element into four smaller

elements. The refined meshes considered in this test are meshes with h=0.5 (77 nodes), h=0.25 (273 nodes), and h=0.125 (1025 nodes). The K-FEM options used for analyses of the beam and the other following problems are: P2-2-G80, P2-2-QS, P3-3-G80, and P3-3-QS.

Plots of relative error norms for displacement and strain energy and their convergence rates are shown in Figs. 8 and 9, respectively. The fastest convergence rate for displacement is achieved for the K-FEM with P2-2-QS (the convergence rate R=1.94). The three other options result in nearly the same rate (around 1.5). In terms of strain energy error norm, all of the K-FEM options converge with nearly the same convergence rate (around 1). The K-FEM with P3-3-G80 is the most accurate one. It is worthwhile to note that in this problem the K-FEM with cubic polynomial basis should theoretically reproduce the exact solutions because the order of the exact solutions is three. However this is not the case here because of inter-element *non-conformity* of the K-FEM with P3-3.

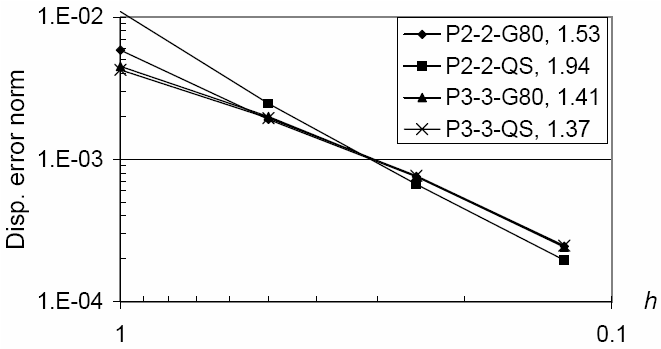

Fig. 8 Relative errors of displacement norm and convergence rates for the beam

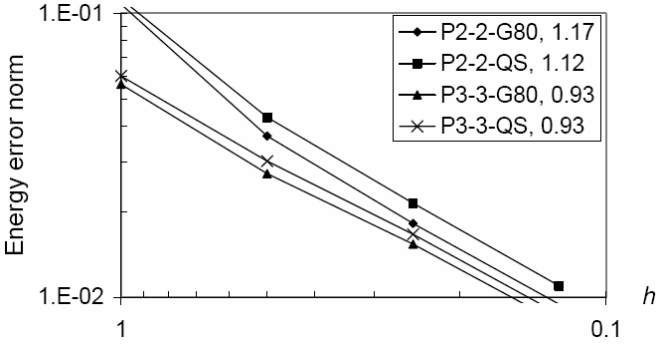

Fig. 9 Relative errors of strain energy norm and convergence rates for the beam

The contours of the normal stress in x direction, σ_x, and the shear stress, τ_x, without averaging process, are displayed in Fig. 10 for the mesh with h=0.5 and the K-FEM options P3-3-QS. These plots demonstrate the capability of the K-FEM to produce smooth stress distributions in a relatively course mesh. The average nodal shear stresses of the beam at the mid-span are shown in Fig. 11 for the mesh with h=0.25 and the options P2-2-QS and P3-3-QS. The figure demonstrates the accuracy of the method in computing the shear stress, which is generally hard to obtain for the standard FEM. The K-FEM with P3-3-QS is slightly more accurate than that with P2-2-QS, particularly at the edges of the beam.

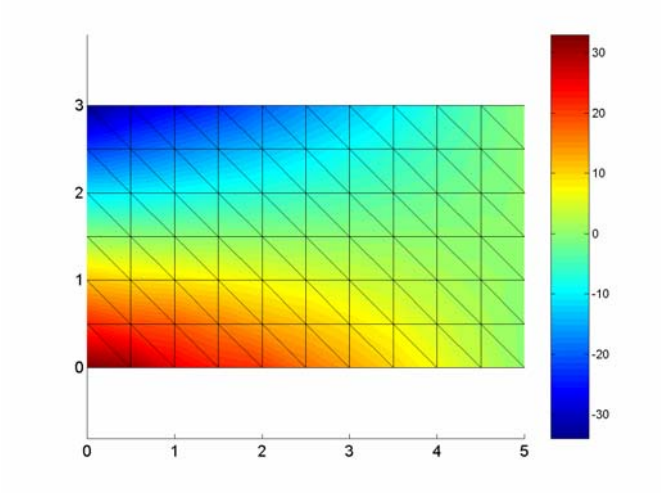

(a) Normal stress, σ_x

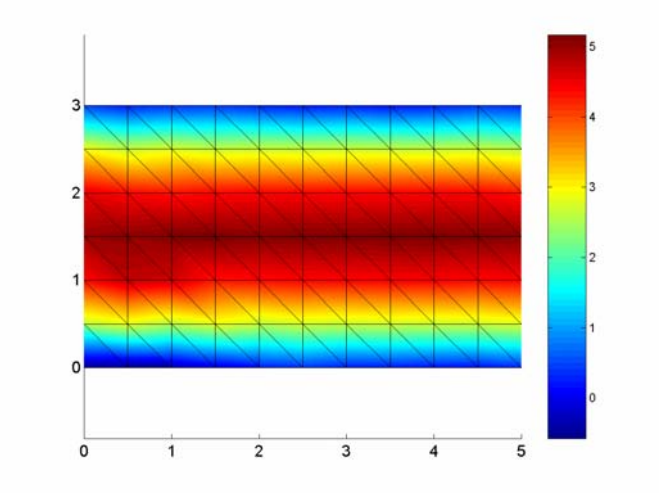

(b) Shear stress, τ_{xy}

Fig. 10 Un-averaged stress contours for the cantilever beam discretized with 6-by-10 mesh with P3-3-QS

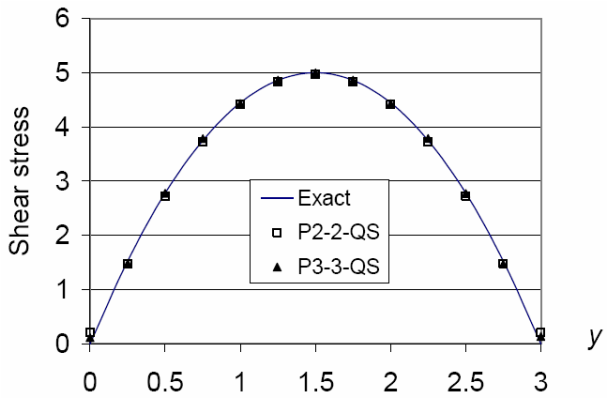

Fig. 11 Average shear stresses at the mid-span of the cantilever beam with mesh of h=0.25

An Infinite Plate with a Hole

An infinite plane-stress plate with a circular hole of radius a=1 is subjected to a uniform tension T_x=100 at infinity [16] (Fig. 12). The exact stress fields in the plate are given as follows [15]:

$$\sigma_x = T_x\left[1-\frac{a^2}{r^2}\left(\frac{3}{2}\cos 2\theta+\cos 4\theta\right)+\frac{3a^4}{2r^4}\cos 4\theta\right] \tag{25a}$$

$$\sigma_y = T_x\left[-\frac{a^2}{r^2}\left(\frac{1}{2}\cos 2\theta-\cos 4\theta\right)-\frac{3a^4}{2r^4}\cos 4\theta\right] \tag{25b}$$

$$\tau_{xy} = T_x\left[-\frac{a^2}{r^2}\left(\frac{1}{2}\sin 2\theta+\sin 4\theta\right)+\frac{3a^4}{2r^4}\sin 4\theta\right] \tag{25c}$$

where r and θ are the polar coordinates and θ is measured from the positive x-axis counter-clockwise. Owing to symmetry, only the upper right quadrant of the plate, $0 \le x \le 5$ and $0 \le y \le 5$, is analyzed. Zero normal displacements are prescribed on the symmetric boundaries and the traction boundary conditions given by the exact stress, Eqs. (25a)-(25c), are imposed on the right (x=5) and top (y=5) edges.

The initial course mesh of 42 nodes is shown in Fig. 13. The element characteristic size for this problem is taken as the distance between two nodes at the right or top edge, i.e. h=1. Subsequently, the mesh is refined by subdividing the previous element into four smaller elements. The refined meshes considered in this test are meshes with h=0.5 (141 nodes) and h=0.25 (513 nodes). In performing the analysis with h=0.25 using Gaussian correlation function, the scale factor f=0.79 is used in place of f=0.8 because the use of f=0.8 results in det(**R**) exceeding the upper bound criterion, Eq. (10), for some elements.

The convergences for displacement and strain energy are shown in Figs. 14 and 15, respectively. The rates of convergence of all K-FEM options are nearly equal, for displacement as well as strain energy. The fastest convergence rate in terms of displacement error is achieved by the K-FEM with P3-3-G80 (R=2.60) while the fastest one in terms of strain energy error is the K-FEM with P3-3-QS (R=1.37). Theoretically, the accuracy and convergence rate of the K-FEM with cubic basis are higher than those with quadratic basis. However, this is not the case here because of the nonconformity of the K-FEM.

The contour of the un-averaged normal stress in x direction, σ_x, for the plate with mesh of h=0.5 and the option P3-3-QS is shown in Fig. 16. Again, it demonstrates the capability of the present method to produce smooth stress distribution even for a rather crude mesh.

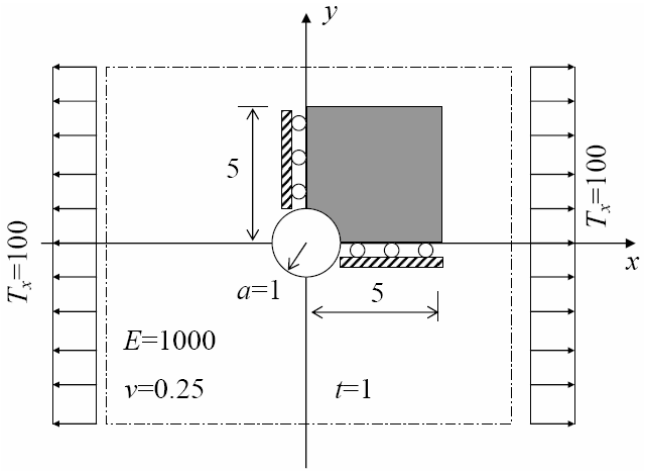

Fig. 12 An infinite plate with a circular hole

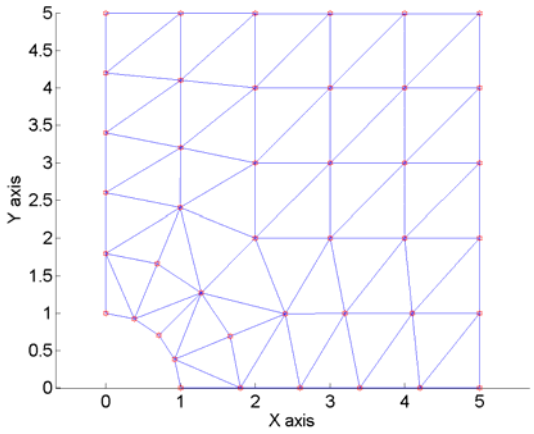

Fig. 13 Initial mesh of the holed plate

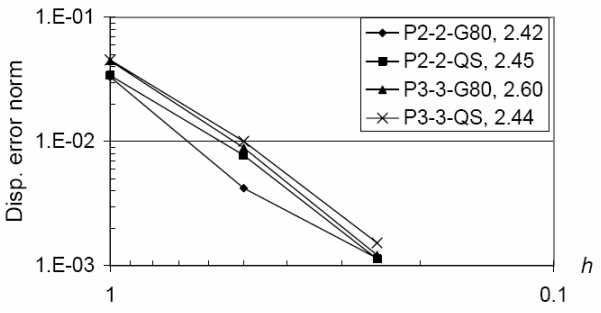

Fig. 14 Relative errors of displacement norm and convergence rates for the holed plate

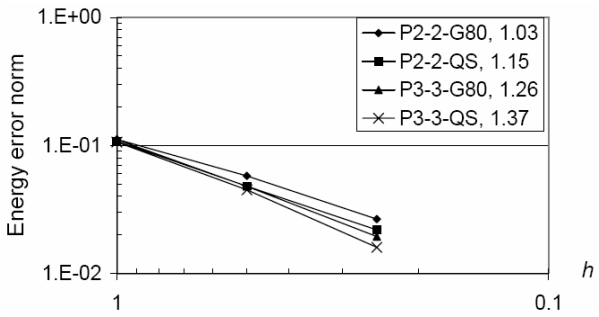

Fig. 15 Relative errors of strain energy norm and convergence rates for the holed plate

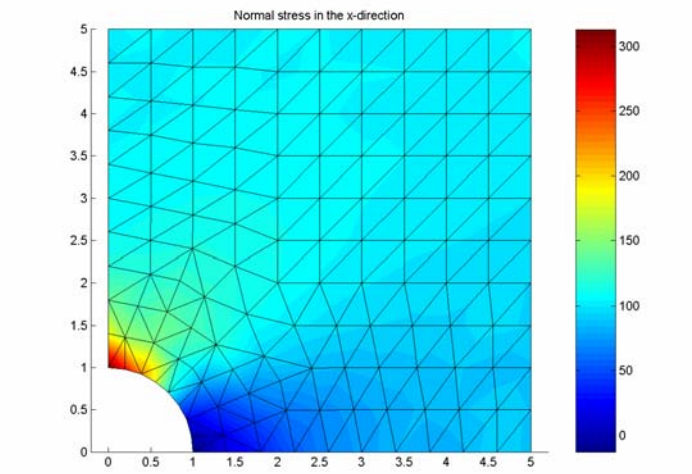

Fig. 16 Contour of un-averaged σ_x for the holed plate discretized with 141 nodes, computed using the K-FEM with option P3-3-QS

The average nodal stresses σ_x along x=0 are depicted in Fig. 17 for the mesh with h=0.25 for two options: P2-2-QS and P3-3-QS. It can be seen that the K-FEM with P2-2-QS gives a reasonably accurate stress distribution but there are some fluctuations at the region near the peak stress and at the boundary y=5. The K-FEM with P3-3-QS captures better the steep stress distribution near the peak stress.

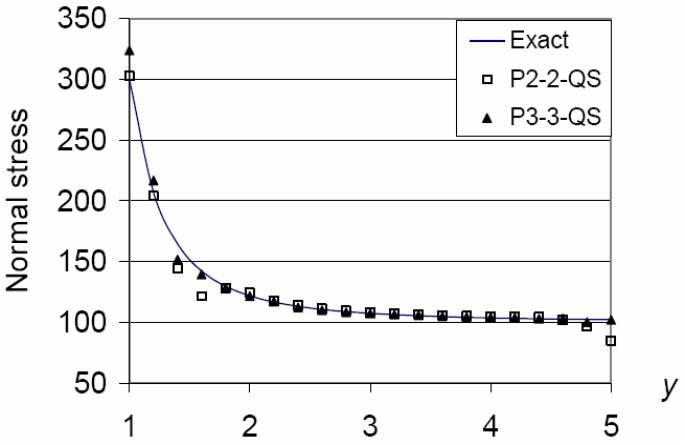

Fig. 17 Normal stress in the x-direction along line x=0 of the holed plate with mesh of h=0.25

CONCLUSIONS

The fundamentals of the K-FEM and its application to two-dimensional elastostatics have been presented. The basic concepts are applicable to many problems in continuum mechanics. Besides the commonly-used Gaussian correlation function, the QS function is introduced as an alternative for the correlation model. The advantage of the use of the QS is that the shape functions are not very sensitive to the change of the parameter. The numerical tests with two benchmark problems in plane-stress/plane-strain problems demonstrate the superior convergence and accuracy of the method.

The present method is as simple as the conventional FEM in terms of the formulation and implementation yet it is as flexible as mesh-free methods. The drawback of the present method is that it is non-conforming along inter-element boundaries. However, despite the non-conformity, the numerical examples showed very good convergence characteristics. Future researches may be directed at: (1) extension and application of the K-FEM to different problems in engineering, (2) inclusion of adaptive mesh refinement, (3) improvement of the computational efficiency in constructing Kriging shape functions.

REFERENCES

[1] G. R. Liu, *Mesh Free Methods*, CRC Press, Boca Raton, USA (2003).

[2] Y. T. Gu, *Meshfree methods and their comparisons*, Int. J. Comput. Meth., 2, (2005), 477-515.

[3] T. Belytschko, Y. Y. Lu, L. Gu, *Element-free Galerkin methods*, Int. J. Num. Meth. Eng., 37, (1994), 229-256.

[4] K. Plengkhom, W. Kanok-Nukulchai, *An enhancement of finite element methods with moving Kriging shape functions*, Int. J. Comput. Meth., 2, (2005), 451-475.

[5] L. Gu, *Moving Kriging interpolation and element-free Galerkin method*, Int. J. Num. Meth. Eng., 56, (2003), 1-11.

[6] F. T. Wong, W. Kanok-Nukulchai, *Kriging-based finite element method for analyses of Reissner-Mindlin plates*, in W. Kanok-Nukulchai, S. Munasinghe, N. Anwar eds. *Emerging Trends*: *Keynote Lectures and Symposia. Proc. 10th East-Asia Pacific Conf. Struct. Eng. Const.*, *Bangkok*, *3-5 August 2006*, ACECOMS, Pathumthani, Thailand (2006), pp. 509-514.

[7] C. Wicaksana, W. Kanok-Nukulchai, *Dynamic analysis of Timoshenko beam and Mindlin plate by Kriging-based finite element methods*, in W. Kanok-Nukulchai, S. Munasinghe, N. Anwar eds. *Emerging Trends*: *Keynote Lectures and Symposia. Proc. 10th East-Asia Pacific Conf. Struct. Eng. Const.*, *Bangkok*, *3-5 August 2006*, ACECOMS, Pathumthani, Thailand (2006), pp. 515-524.

[8] W. Sommanawat, W. Kanok-Nukulchai, *The enrichment of material discontinuity in moving Kriging methods*, in W. Kanok-Nukulchai, S. Munasinghe, N. Anwar eds. *Emerging Trends*: *Keynote Lectures*

and Symposia. *Proc. 10th East-Asia Pacific Conf. Struct. Eng. Const.*, *Bangkok*, *3-5 August 2006*, ACECOMS, Pathumthani, Thailand (2006), pp. 525-530.

[9] Z. Masood, W. Kanok-Nukulchai, *An adaptive mesh generation for Kriging element-free Galerkin method based on Delaunay triangulation*, in W. Kanok-Nukulchai, S. Munasinghe, N. Anwar eds. *Emerging Trends*: *Keynote Lectures and Symposia*. *Proc. 10th East-Asia Pacific Conf. Struct. Eng. Const.*, *Bangkok*, *3-5 August 2006*, ACECOMS, Pathumthani, Thailand (2006), pp. 499-508.

[10] R. A. Olea, *Geostatistics for Engineers and Earth Scientists*, Kluwer Academic Publishers, Boston, USA (1999).

[11] H. Wackernagel, *Multivariate Geostatistics*, 2nd edition, Springer, Berlin, Germany (1998).

[12] F. T. Wong, W. Kanok-Nukulchai, *On the convergence of the Kriging-based finite element method*, to be presented in *APCOM'07 in conjunction with EPMESC XI*, *Kyoto*, *3-6 December 2007*, *JAPAN*.

[13] H. Noguchi, T. Kawashima, T. Miyamura, *Element free analyses of shell and spatial structures*, Int. J. Num. Meth. Eng., 47, (2000), 1215-1240.

[14] T. J. R. Hughes, *The Finite Element Method: LinearStatic and Dynamic Finite Element Analysis*, Prentice-Hall, New Jersey, USA (1987).

[15] S. N. Atluri, T. Zhu, *New concepts in meshless methods,* Int. J. Num. Meth. Eng., 47, (2000), 537-556.

[16] P. Tongsuk, W. Kanok-Nukulchai, *Further investigation of element-free Galerkin method using moving Kriging interpolation*, Int. J. Comput. Meth., 1, (2004)**,** 345-365.